Fuel 383 (2025) 133785

Contents lists available at ScienceDirect

Fuel

journal homepage: www.elsevier.com/locate/fuel

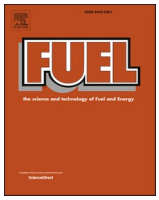

Full Length Article

Characterization of cellular structure appearance in ethanol expanding spherical flames

R. Sastre [a,*], M. Reyes [a], J.M. Rodríguez-Díaz [b], J. Lacey [c]

[a] Department of Energy and Fluid Mechanics Engineering, University of Valladolid, 47011 Valladolid, Spain
[b] Department of Statistics-IUFFyM, University of Salamanca, 37008 Salamanca, Spain
[c] Department of Mechanical Engineering, KU Leuven, 3001 Leuven, Belgium

ARTICLE INFO

Keywords:
Ethanol
Cellularity
Self-acceleration
I-optimal design of experiments
Cellular parameters
Burning velocity

ABSTRACT

The objective of this work is to characterize the combustion process of ethanol flames under cellular conditions. Ethanol is considered an alternative fuel and can be used to replace fossil fuels. To investigate the behavior of ethanol as a fuel, some of its combustion properties are measured and characterized, such as laminar burning velocity and flame front stability, which strongly depend on the appearance of cellularity on the flame. The study is developed in a cylindric constant volume combustion bomb instrumented with Schlieren technique to visualize ethanol flames and make an optical diagnosis of the combustion process. Some cellular parameters are proposed to characterize the cellular structure of the flame, which quantitatively define the appearance and cellularity development, such as cellular radius, the time for the cellular structure apparition on the flame and the influence of cellularity on the burning velocity. Other dimensionless parameters that can help to determine the influence of cellularity in the combustion process and compare between different flames. An I-Optimal design of experiments is proposed in this work to characterize the flame stability of ethanol, design the experimental testing and develop predictive models for the proposed cellular parameters. The proposed area of study to assure cellular flames is delimited by an initial temperature of 343K, initial pressures from 0.15 MPa to 0.30 MPa and equivalence ratios ranging from 0.8 to 1.4. Images confirm that models predict correctly the cellular radius and others cellular parameters, and the appearance of cellularity affects the burning velocity generating an auto-turbulence in the flame which enhance it. Predictions of cellular radius obtained with developed model are in accordance with the results obtained by other works.

1. Introduction

Due to concerns about global warming and environmental contamination there are a growing interest in investigating in renewables as alcohols. This is particularly important in the transportation sector due to the use of Internal Combustion Engines (ICE), which currently rely almost exclusively on fossil fuel streams. There are several pathways possible for decarbonized replacement fuel: one of them is to use zero-carbon fuels, such as hydrogen H_2 or ammonia NH_3 produced from renewable energy sources. Several researchers have developed works about the behavior of such fuels, e.g. [1–7]. An alternative method is to use carbon-based fuels obtained from organic feedstocks, such as biomass and organic waste. This is the case of the bioethanol or ethanol derived from cultivation rich in cellulose (e.g. sugar or corn). The advantage of using bioethanol in an ICE is that the CO_2 that it generates was previously captured by the plants that generated this alcohol, and thus, this fuel has net-zero carbon emissions, contributes to a circular economy and enhances the primary sector [8,9].

To characterize the stability of a combustion process, a Constant Volume Combustion Bomb (CVCB) could be employed. This kind of facility enables to study and analyze the combustion isolated under laminar conditions — that is, without external turbulence —. The combustion stability of the fuel determines the influence of certain phenomenon, referred to as flame front instabilities, in the development of the combustion event [10]. The combustion stability can be significant for the morphology and topology of the flame because when the flame front instabilities are sufficiently large, they change the structure of the flame front which can generate cellularity. This cellularity phenomenon also impacts the burning velocity (u_n). This is the relative speed at which the unburned gas (fuel and air) moves towards the flame front when there is no external turbulence that influence the process, with the

* Corresponding author.
E-mail address: rosaura.sastre@uva.es (R. Sastre).

https://doi.org/10.1016/j.fuel.2024.133785
Received 10 July 2024; Received in revised form 15 November 2024; Accepted 18 November 2024
Available online 1 December 2024

Nomenclature

Latin symbols

T	Temperature [K]
r	Radius [m] or [cm]
A	Area [m2] or [cm2]
m	Mass [kg] or [g]
Sn	Flame propagation speed [m/s]
u_n	Stretched laminar burning velocity [m/s]
u_l	Unstretched laminar burning velocity [m/s]
u	Burning velocity [m/s]
p	Pressure [MPa]

Greek symbols

ρ	Density [kg/m^3]
φ	Fuel/air equivalence ratio
ξ	Experimental design
β	Vector of unknown model parameters
ε	Random error
σ	Standard deviation of random error

Subscript symbols

Cell	Cellular
Comb	Combustion
max	Maximum
i	Initial condition
f or flame	Referred to the flame
l	Referred to a unstretched laminar flame
b	Referred to the gas burned
ub	Referred to the unburned gas
n	Referred to a stretched laminar flame

Acronyms

LBV	Laminar Burning Velocity [m/s]
CVCB	Constant Volume Combustion Bomb
ICE	Internal combustion engine
CCS	Cellular Combustion Stage
RoUBV	Rate of unaffected burning velocity

reference system located in the flame front itself. For an ideal planar flame, the laminar burning velocity is denoted by u_l and, contrary to the spherical flame, it is not influenced by the flame curvature, i.e., it is unstretched. The laminar burning velocity depends on the burned mass flow rate, the density of the unburned gas and the flame front area ([3,11]) as it is expressed in: $u_n = \frac{\dot{m}_b}{\rho_u \bullet A_f}$.

The initial flame kernel growth is governed by the laminar burning velocity, even after the flame kernel development, the burnup rate of turbulent eddies is also governed by it. There are many ways to calculate the laminar burning velocity of a fuel; one of them is by using the afore mentioned CVCB, where a combustion process occurs, which generally develops an approximately spherical flame front, as the work developed by Reyes et al. [12] that aimed to calculate the laminar burning velocity of premixed methane-air and hydrogen-air mixtures in a CVCB at moderate pressure and temperature. In this study, the data of the beginning and end of the combustion event were discarded. The first group of data was removed because of the noise caused by the spark at the beginning of the process; the second group of data was removed because of the superimposition of the cellularity phenomena. The cellularity caused an apparent burning velocity larger than the laminar one, i.e., the process accelerated due to the augmentation of the burned mass flow rate (the wrinkling increases the area of the flame front), which is also explained by Hu et al. [13]. This is called the self-acceleration phenomenon and there are several recent studies that show this same influence of the instabilities in the laminar burning velocity (u_n) and in the flame speed (S_n), see [14–17]. The flame speed is the velocity at which the flame is progressing with respect to the chamber walls ($S_n = \frac{dr}{dt}$). Burning velocity (u_n) and the flame speed (S_n) are related, $u_n = \frac{\rho_b}{\rho_u} S_n = \frac{\rho_b}{\rho_u} \frac{dr}{dt}$.

Understanding the self-acceleration phenomenon and the appearance of cellularity (or lack thereof) is connected to flame stability analysis, which refers to the identification of the origin and growth of the instabilities inherent to a combustion process. These instabilities are caused mainly by thermo-diffusive and hydrodynamic effects, but also by volumetric forces under certain conditions of pressure and temperature. Intrinsic instabilities are predominant in thermal engines, and they can increase the working efficiency and can cause end-gas auto-ignition [18–20]. Fundamental combustion parameters such as burning velocity, combustion performance, flame front morphology and flame front thickness are impacted by these instabilities and the appearance of cellularity, affecting the development of the combustion.

The influence of the instabilities generated in the flame front in the combustion event has been studied by many authors in the last decades, starting with the works of Markstein [21], who carried out an investigation regarding flame stability, as well as Istratov and Librovich. Researchers continued developing the instabilities theory as Clavin in 1985 [22], Williams in 1985 [23], Betchtold and Matalon in 1987 [24], Bradley in 2000 [25], Addabbo in 2001 [26], Law et al. in 2005 [27] and others [19,28–30], growing the interest in this topic until recent years when new studies have been developed based on these previous investigations [20,31–38].

Hinton [39] proposed a stable basis for the development of the cellular detection with pressure evolution through a graphical evaluation between the image analysis and the pressure evolution: the second time derivative of the pressure and the number of edges due to the cellularity. In a two zones thermodynamic model, the burning velocity of a combustion process is directly related to the derivative of pressure with respect to time (see the two zones thermodynamic model developed by Giménez et al. [40]). Burning velocity evolution may be considered a link between the pressure measured and the detection of a cellular flame front.

Studies related to the instabilities in combustion processes have been recently published not only for ethanol/air blends but also for blends of ethanol with other fuels. Gárzon et al. [41] investigated the ethanol/air combustion process and the influence of water-addition in hydrous ethanol flame front instabilities at different temperatures and pressures. They concluded that the equivalence ratio has a significant effect on flame stability: in slightly rich mixtures they found the maximum tendency for hydrodynamic instabilities; on the contrary, richer combustion processes ($\Phi >> 1$) have greater tendency to develop thermal-diffusive instabilities. The initial pressure also enhances the thermal-diffusive instability type, especially on the rich side. Nevertheless, the initial temperature has a smaller influence in the development of the instabilities of the flame front. These conclusions are in accordance with those presented in a previous study carried out by Zhang et al. [35], in which a numerical and theoretical analysis of ethanol/air flame instabilities was presented.

Li et al. [31] examined the influence in the flame instability of the hydrogen content in hydrogen/ethanol/air combustion processes. Likewise, Liu et al. [36] analyzed the influence of initial temperature and pressure in E30 (30% ethanol and 70% gasoline on volume basis)/air flames stability as well as the type of instabilities that developed in each condition.

In most scientific fields, experimental designs are conducted with the purpose of a better understanding of the appearance of cellularity during

the evolution of a laminar flame. Usually, the aim of the experimental design is to estimate the relationship between a variable of interest (response variable, which is a dependent variable) and others that are under the control of the operator (factors, which are independent or explanatory variables). The idea is to study the variation of the response variable due to changes in the values of the independent variables, usually trying to estimate well the model relating the variables or attempting to derive accurate predictions of the value of the response variable for a specific set of factors.

The number of experimental tests that is possible to perform is limited due to temporal, economic and/or other different reasons, thus it is essential to choose carefully the most informative conditions where observations are to be taken, that is, the combinations of values of the independent variables and factors that will provide the best knowledge about the object of study, within the budget restrictions. In other words, to choose the optimal design for the experiment, a procedure should be followed in the first steps of the process before taking the observations or experimentations.

For that reason, the main objective of the experimental design is to find the optimal conditions where observations should be taken in order to obtain the maximum information. Two main approaches can be followed: the first one consists of getting the best estimate of the model parameters, that is, the estimators with minimum variance, and the second one consists of trying to minimize the variance of the prediction of the response. Due to the fact that the inverse of the information matrix is proportional to the covariance matrix of the estimators of the model parameters, optimal designs typically minimize some convex function of the inverse of the information matrix. For non-linear models, the latter will depend on the initial values or distributions of the model parameters, as do the optimal designs. Thus, the procedure will provide locally optimal designs, that are good for (or near) the initial values of the parameters.

The choice of the function to minimize depends on the objectives of the operator and will lead to the different optimality criteria. For the first approach to estimate the parameters of the model, the advisable criterion is D-optimality, that focuses on the determinant of the information matrix. A design ξ is D-optimal if maximizes this determinant, which is equivalent to minimizing that of the covariance matrix. Another popular alternative is A-optimality that considers the trace of the covariance matrix, thus minimizing the average of the variances of the model parameters estimators. There are two of the Characteristic Criteria defined in the work developed by López-Fidalgo and Rodríguez-Díaz [42–44]. When the objective is to estimate a specific parameter or a linear combination of them, C-optimality should be employed. The corresponding optimal designs can be computed geometrically using Elfving's Theorem [45], mainly used for two-parameter models. Later on, the procedure was extended for models with more parameters [46] and correlated observations [47].

Regarding the second approach, that is optimizing the prediction of the response, the appropriate criteria is C-optimality, which minimizes the maximum of the prediction variance in the design space, or I-optimality, which considers instead the mean of the prediction variance. Either approach requires knowledge of the analytical expression of the model (linear or non-linear); when it is not possible to obtain such an expression, a procedure like the one described in Rodríguez-Díaz and Sánchez-León in 2014 [48] can be employed. For more information see references [49–51].

This work aims to study alcohol fuels, ethanol in particular, to replace fossil fuels such as gasoline or diesel. To understand the behavior of ethanol as a fuel, it is necessary to measure and to characterize some of its combustion properties, such as the burning velocity and flame front stability, which strongly depend on the appearance of cellularity on the flame. A D-optimal design of experiments is proposed in this work to characterize the flame stability of ethanol. Although there are several works that characterize the instabilities in the flame front of ethanol combustions processes [31,35,52] there are no studies that apply this type of experimental methodology (optimal designs) to study flame instability and cellularity for alternative fuels. In particular, the optimal design is proposed to obtain models for quantifying parameters that could characterize the cellularity phenomenon in the flame front. These parameters are also established and defined in this work.

2. Experimental methodology

The experimental methodology used in this research work is described in four different parts: initially, it is presented a short description of the experimental facility used in this work; secondly, the cellular parameters selected to investigate the cellularity apparition in the flame front are explained; thirdly, the determination of the area of study to assure cellular ethanol flames, in terms of initial conditions of pressure, temperature and fuel/air equivalence ratio is detailed; and finally, it is detailed the overall methodology used to obtain the values of the defined parameters is explained.

2.1. Experimental setup

In this work, the ethanol/air flames are characterized in a CVCB for studying the cellularity phenomena on the flame. The CVCB is a combustion chamber with cylindrical geometry with a diameter of 114 mm and 135 mm of length [3]. This combustion bomb is used to investigate the combustion development under premixed conditions as shown in Fig. 1. The combustion chamber has with two optical windows made of fused silica on the sidewalls of the cylinder. The experimental installation is instrumented to measure instantaneous pressure using a piezoelectric pressure transducer Kistler type 7063, and it is also prepared to visualize the flame development with a high-speed Schlieren technique system, through which flame images are recorded using a high-speed camera Phantom V210 at 7000 frames per second (resolution 832 × 800 and exposure time of 10 ms), more details can be found in a previous work [53].

Ethanol is introduced with micro syringes, and air is introduced using the partial pressures method. Once the reactants are introduced, and the initial conditions of pressure and temperature are fixed, an ignition system starts the combustion at the center of the combustion chamber. When the combustion is induced, a flame front develops and propagates spherically inside the CVCB, while the unburned mixture is compressed and burned. The mixture is left to stand for five minutes to ensure thorough pre-mixing. To ensure the accuracy and repetitively of the experimental results, each condition is tested at least three times to minimize the impact of any single experiment.

For image processing, an in-house developed algorithm in Python Open CV is used to analyze the images obtained with the high-speed camera and to determine the flame radius evolution. Radius evolution is analyzed through frame-by-frame processing, after background removal, binarization and thinning transformation to highlight the borders, as explained in detail in Tinaut et al.[3]. The image processing finds the position of the flame front during the combustion development and measures the instantaneous radius and the cellular density. The Python algorithm is used for the optical processing of the images obtained with the high-speed camera using Schlieren technique. With this procedure, it is possible to obtain the time evolution of the flame front and the flame radius through frame by frame processing. The algorithm calculates the radius in each Schlieren image, providing the instantaneous position of the flame front. An algorithm called RANSAC is used to recognize the flame front and calculate the radius of the average circumference associated to the flame in each image.

2.2. Response variables: Selection of the parameters that characterize the cellularity

In the second part of the methodology, some representative parameters, Cellular Parameters, are used to describe the cellular behavior of

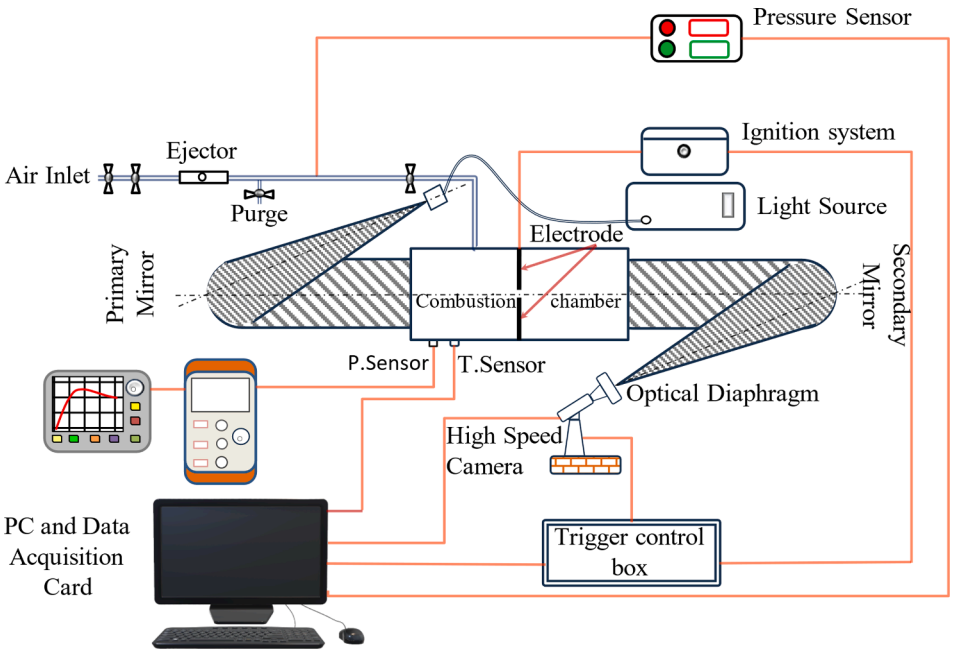

Fig. 1. Scheme of the experimental setup.

ethanol flames and are explained in this section.

The instabilities growth is related to both physical and thermodynamic factors, and there are several possible parameters that could characterize it. We have selected six cellular parameters: four dimensional and two dimensionless parameters. The first is the *cellular trigger time* (t_{trigg_cell}), the time at which the burning velocity starts to be significantly affected by the instabilities growth. This is a consequence of the flame surface increase due to the instability progress [25,54]. The second cellular parameter is the cellular radius (r_{cell}), that means the flame radius that corresponds to the cellular trigger time. The cellular radius has been a reference parameter in the study of cellular flames (sometimes is also denominated as "*cellular radius*") [55–57]. The third selected cellular parameter is the *time at which the maximum burning velocity is reached* (t_{max}), i.e., the moment at which the burning velocity is most affected by the cellularity. A two-zone thermodynamic model was applied to calculate the instantaneous stretched laminar burning velocity (un(t)) for each experiment (for more information see [12,58]). The fourth cellular parameter is *combustion duration* (t_{comb}), which is associated with the time for maximum pressure, when the flame front hits the walls and the combustion process is completed. The fifth is a dimensionless cellular parameter, the *Ratio of Unaffected Burning Velocity (RoUBV)* which represents the time that the burning velocity is unaffected by cellularity compared with the time at which the velocity is most affected, that is, when the burning velocity attains its maximum value. And the sixth, which also is a dimensionless cellular parameter, the *Cellular Combustion Stage (CCS)* defined as the period that the instabilities (cellularity) affect the combustion process compared to the total duration of the combustion process, i.e., the instant at which the maximum pressure is reached. RoUBV and CCS give important information, such as if the instabilities occur during an early or a late stage of the combustion process. This information is reflected in the values of those parameters, because the higher they are, the later the influence of instabilities will take place, and vice versa. All the cellular parameters previously detailed to characterize the combustion progress and cellularity development are summarized in Table 1.

Table 1
Cellular parameters to characterize the combustion progress and cellularity development.

	Dimensional parameters	
	Name, symbol [units]	Definition
1	Cellular trigger time, t_{trigg_cell} [ms]	Trigger time that takes the instabilities to affect the burning velocity, or Instant at which the combustion velocity starts to be significantly affected by the instabilities growth (cellularity).
2	Cellular radius, r_{cell} [cm]	The flame radius corresponding to the cellular trigger time.
3	Maximum burning velocity time, t_{ul_max} [ms]	Instant at which the combustion process reaches the maximum burning velocity.
4	Combustion time, t_{comb}, [ms]	Total duration of the combustion process.
5	Ratio of Unaffected Burning Velocity, RoUBV	Percentage of the burning velocity unaffected by cellularity compared to the maximum burning velocity time. $RoUBV = \frac{t_{trigg\_cell}}{t_{max}}$ Eq. [1]
6	Cellular Combustion Stage, CCS.	Fraction of combustion process affected by cellularity. $CCS = 1 - \frac{t_{cell}}{t_{comb}}$ Eq. [2]

2.3. Establishing the area of study for the cellularity characterization

In this part of the methodology, it is explained how is obtained the area of study with the objective of studying the instabilities development in ethanol flames and to assure cellular flames. For this purpose, raw limits of pressure and equivalence ratio between which the cellularity phenomenon occurs are initially considered for a given initial temperature of 343 K. With this initial temperature it is possible to get a bigger study area to investigate the cellularity apparition. A series of experiments was carried out to define those limits that constitute the approximate area of study, and which are represented in Fig. 2, based on the studies of Garzón Lama [41], pressure enhances the instabilities development, i.e., for a higher initial pressure level, wider equivalence ratio limits could be considered. In that investigation they also concluded that the temperature had a weaker effect on the instabilities development. As ethanol is a carbon-based fuel, it develops combustions instabilities for equivalence ratios on the rich side or slightly lower than the stoichiometric one [19,41].

In Fig. 2, the conditions of initial pressure and equivalence ratio for the selected experiments are presented, as well as the area of study

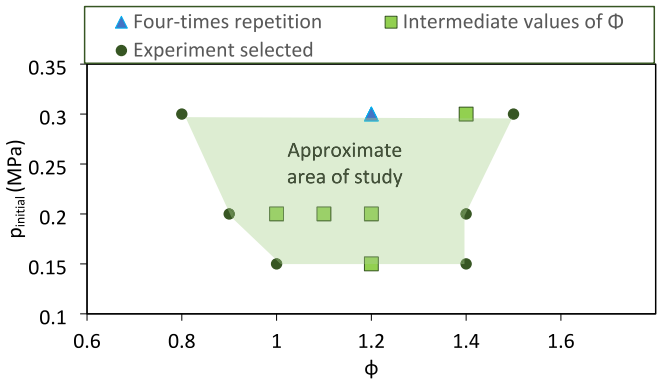

Fig. 2. Pilot series and approximate area of study, which highlights the approximate cellularity limits for ethanol for 343K.

delimited by these conditions. The lower limits for the equivalence ratio at different pressures are marked by the appearance of the cellularity in the flame front, though lower equivalence ratios do not significantly promote cellularity. The upper limits of equivalence ratio at different pressures were defined by the appearance of buoyancy. That is, higher equivalence ratios caused an upwards displacement of the flame front provoking its deviation from the spherical flame front. Low initial pressure limits were set according to the lack of cellularity on the surface of the flame front, while high initial pressure limits depended on the endurance of the facilities to withstand the maximum pressures. This area of study is important because it is an input to the DoE developed in the following sections.

2.4. Calculation of t_{trigg_cell}, r_{cell}, t_{max}, t_{comb}, RoUBV, and CCS

Once the area of study is defined, the six cellular parameters can be determined. The cellular trigger time (t_{trigg_cell}), which represents the activation time required for the consequences of cellularity on the burning velocity to become evident, can be determined as it is expressed in Fig. 3i, where the temporal evolution of the burning velocity is illustrated. Initially, a basic linear regression of the combustion rate is performed, excluding the early combustion regions affected by spark noise and initial disturbances, as well as the cellular region where the burning velocity deviates from the non-cellular laminar burning velocity. This serves as the base parameter for calculating the remaining cellular parameters.

The cellular radius (r_{cell}) is directly carried out by means of the cellular trigger time, since it corresponds to the radius of the flame front when the combustion reaches the t_{trigg_cell}, as it is presented in Fig. 3ii. Maximum burning velocity time (t_{max}) is defined as the time at which the maximum burning velocity is reached, as it is represented in Fig. 3i.

The combustion time (t_{comb}), or duration of the combustion process inside the combustion bomb, delimited by time for the maximum pressure, and it is determined as it is shown in Fig. 3iii [63]. Ratio of Unaffected Burning Velocity (RoUBV) and Cellular Combustion Stage (CCS) are calculated for each experiment and obtained results were crucial for a first verification of the cellularity influence. In Fig. 3i are explained the procedure to calculate the cellular trigger time (t_{trigg_cell}) and maximum burning velocity time, t_{ul_max}, based on the percentage of the burning velocity deviation with respect to the unstretched laminar burning velocity from the two-zone model calculation. The dashed line represents the laminar burning velocity that would have ideally the event if there was no cellularity. It was calculated through a linear regression excluding the initial instants of the combustion event (distorted by the initial spark) and the final instants (affected by the cellularity).

The cellular radius (r_{cell}) was calculated with the value of the cellular trigger time (t_{trigg_cell}). The evolution of the flame radius with time is captured through the schlieren technique explained before. The maximum burning velocity time (t_{max}) was calculated similarly to t_{trigg_cell}: the instantaneous laminar burning velocity ($u_n(t)$) was calculated and the instant that corresponded with the maximum value of it was selected as it is shown in Fig. 3i. The combustion duration or combustion time (t_{comb}) is determined with the maximum pressure time, see Fig. 3**ii**.

Results of the six cellular parameters obtained with the experiments carried out to delimit the area of study with cellular flames are presented in Fig. 4 versus the equivalence ratio, along with an uncertainty analysis. Based on these results, predicting the behavior of the cellular parameters in the study area detailed in Fig. 2 is not possible. Therefore, it is necessary to develop an optimal design of experiments through a statistical model to analyze the effect of pressure and equivalence ratio on the cellular behavior of ethanol flames.

3. Design of experiments methodology

In previous section, the experimental methodology is presented, and it is stablished the area of study to assure cellular ethanol flames and made the design of experiments. In this section, firstly, the optimal designs basis is explained and secondly, the best optimal design based on the experimental results obtained for the determination of the area of study is justified (I-optimal) and are proposed the final set of experiments to develop. And finally, it is detailed the predictive statistical models obtained for the considered cellular parameters, which are the response variables of the proposed optimal design.

3.1. Optimal design of experiments

Let $y=F(x,\beta)+\varepsilon$ denote the model expressing the relation between the response and the explanatory variables, where y is the response variable, x is the vector of independent variables, $\beta=(\beta_1,\ldots,\beta_m)^T$ is the vector of unknown parameters, and F(x, β) represents a function that in the general case may be non-linear respect to β. The ε term stands for the random error coming from either the experiment itself or due to a bad choice of the model. Very often it can be known by experience or it may be analytically derived from the problem (for instance from a system of differential equations). An exact design will be a collection of points $\{x_1,\ldots,x_n\}$, of the independent variables, and n is the size of the design.

When dealing with non-linear models, the usual approach is to linearize it and then use the known theory developed for linear models. Therefore, from Fig. 5, linearization appears feasible to capture the observed behavior, and from now, on a linear model $y=f(x)^T\beta+\varepsilon$ will be assumed. In matrix notation it can be expressed as $Y=X\beta+U$, where $Y=(y_1,\ldots,y_n)^T$ denotes the observations vector, U is the residuals vector and $X=(f(x_1)^T,\ldots,f(x_n)^T)$ is the design matrix, with $f\{x)=(f_1(x),\ldots,f_m(x))^T$ and the $f_i(x)$ linearly independent in the experimental domain **X**.

For normally distributed random errors $\varepsilon\equiv N(0,\sigma^2)$, the Least Squares Estimators and the Maximum Likelihood Estimators of the model parameters are the same, which support the use of this method. For independent observations they are given by $\widehat{\beta}=(X^TX)^{-1}X^TY$, with $Var(\widehat{\beta})=\sigma^2(X^TX)^{-1}$. The matrix X^TX is the *information matrix* of the exact design ξ. When the observations are correlated, the Generalized Least Squares estimators should be computed, $\widehat{\beta}=(X^T\sum^{-1}X)^{-1}X^T\sum^{-1}Y$, where $\sum=Var(Y)$ and $Var(\widehat{\beta})=(X^T\sum^{-1}X)^{-1}$, and the information matrix of ξ will be $M(\xi)=X^T\sum^{-1}X$. Furthermore, in this case the traditional estimation of the covariance matrix is biased [59,60] and a correction of the optimality criteria may be considered [61].

In order to compare two designs, ξ and η, that may use a different number of points (n_ξ and n_η respectively) with respect to a specific optimality criterion φ, Equation 3 can be used. This relationship refers to the efficiency of η respect to ξ, provided that the function φ is homogeneous, i.e. $\Phi(k\,M(\xi))=\varphi(M(\xi))/k$. A value greater than 1 would mean that η is better than ξ (and to what extent it is). If a design η has half of

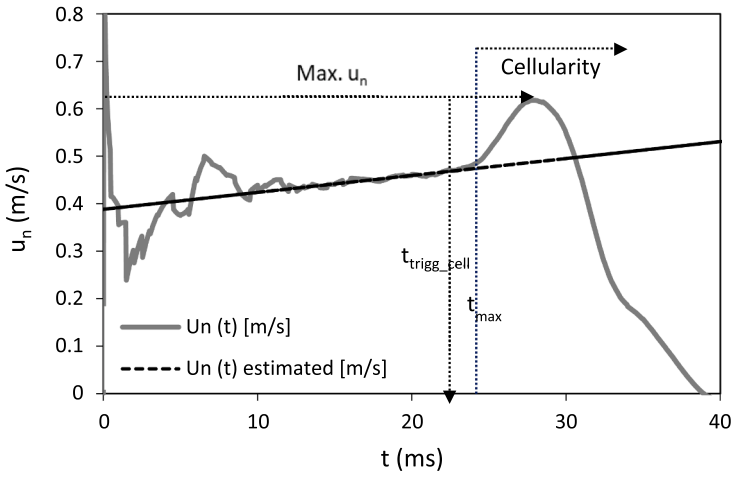

(i) Cellular trigger time ($t_{trigg\_cell)}$ and maximum burning velocity time (t_{ul_max}) determination

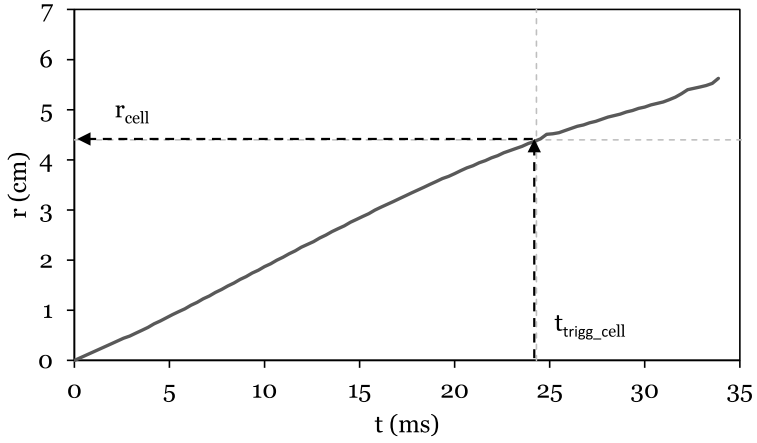

(ii) Temporal evolution of the cellular radius and r_{cell}.

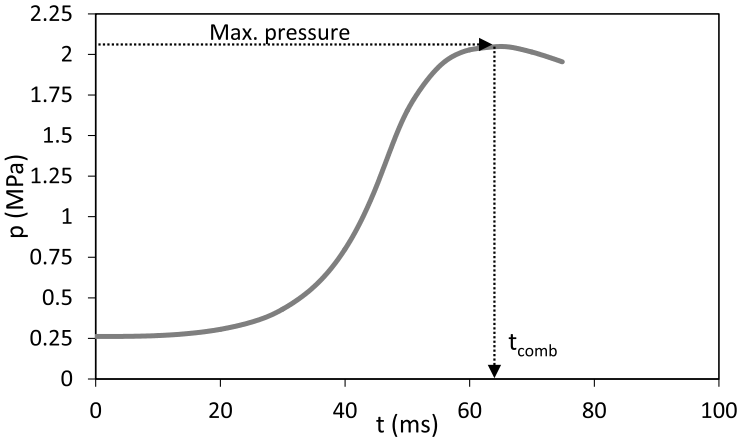

(ii) Combustion time (t_{comb})

Fig. 3. Burning velocity and pressure evolution for ethanol, Φ=0.8; p_i=0.3 MPa; T=343 K.

the efficiency that ξ, that means that when using the design η, one would need two times the number of observations than when using ξ to get the same information (measured by the value of the corresponding optimality criteria). Since the determinant is a non-homogeneous function, for D-optimality the formula that should be employed is presented in Equation 4.

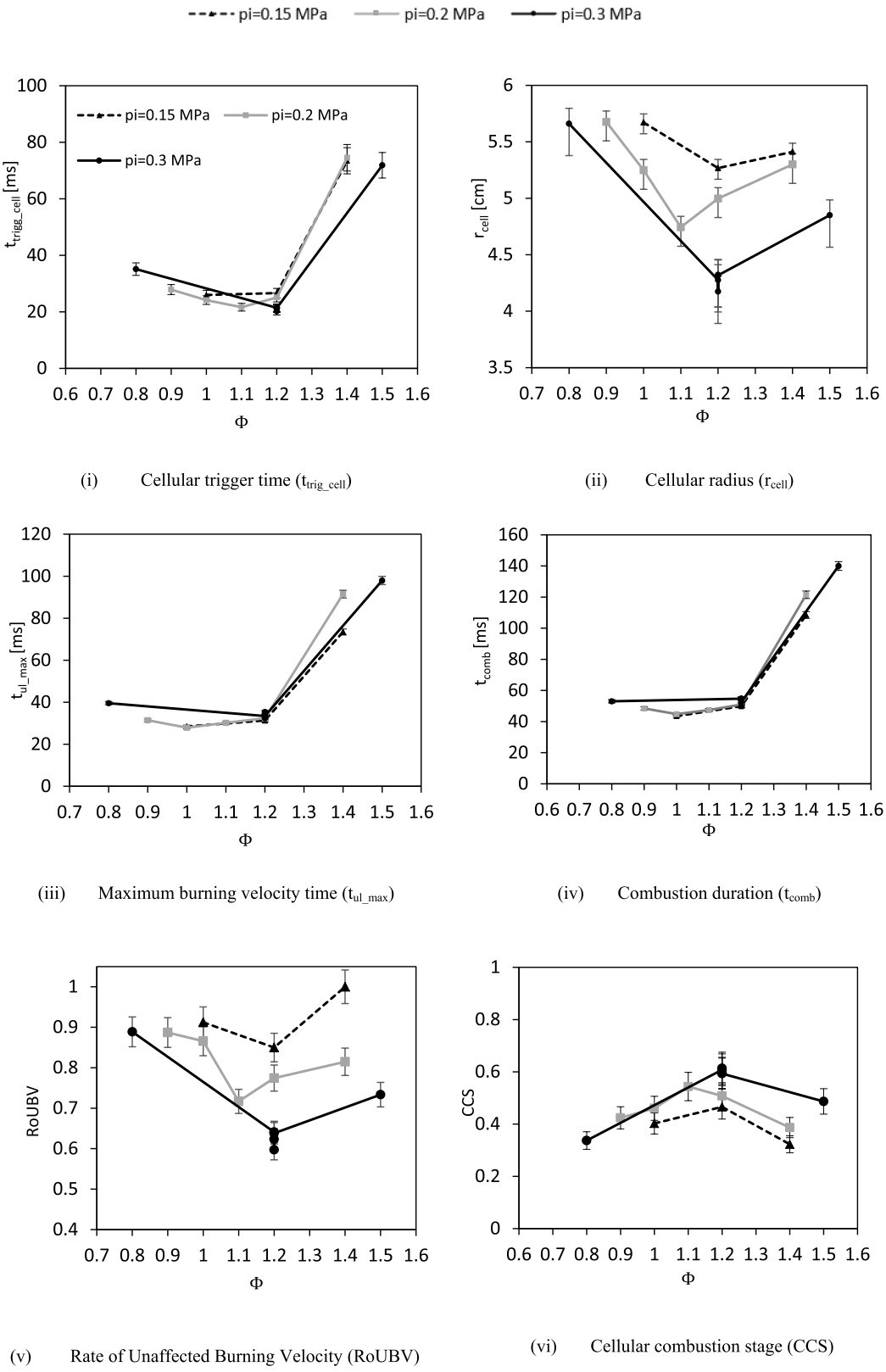

(i) Cellular trigger time (t_{trig_cell})

(ii) Cellular radius (r_{cell})

(iii) Maximum burning velocity time (t_{ul_max})

(iv) Combustion duration (t_{comb})

(v) Rate of Unaffected Burning Velocity (RoUBV)

(vi) Cellular combustion stage (CCS)

Fig. 4. Effect of equivalence ration on the six cellular parameters obtained with the experiments carried out to determine the area of study. Initial Temperature is 343 K and three initial pressures are distinguished by different lines: dotted line is 0.15 MPa, grey line is 0.2 MPa and black line is 0.3 MPa.

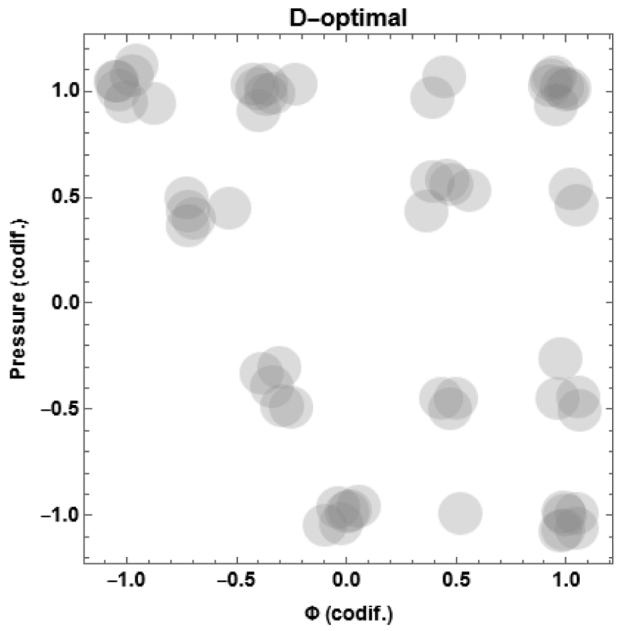

(i) D-Optimal design testing points

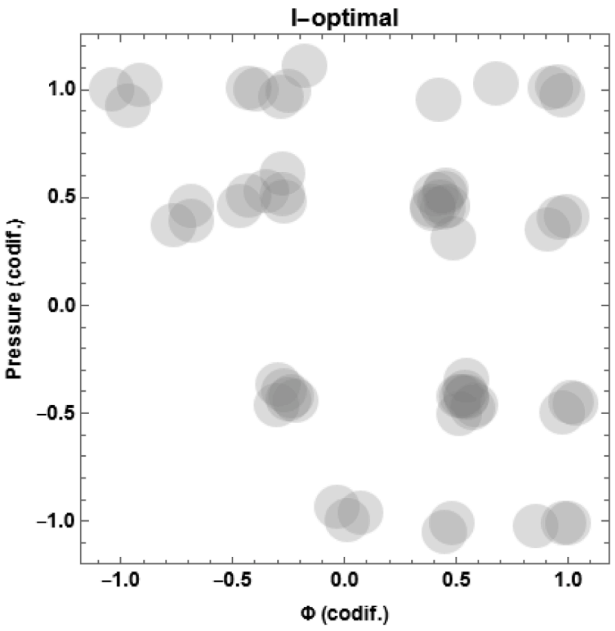

(ii) I-Optimal design testing points

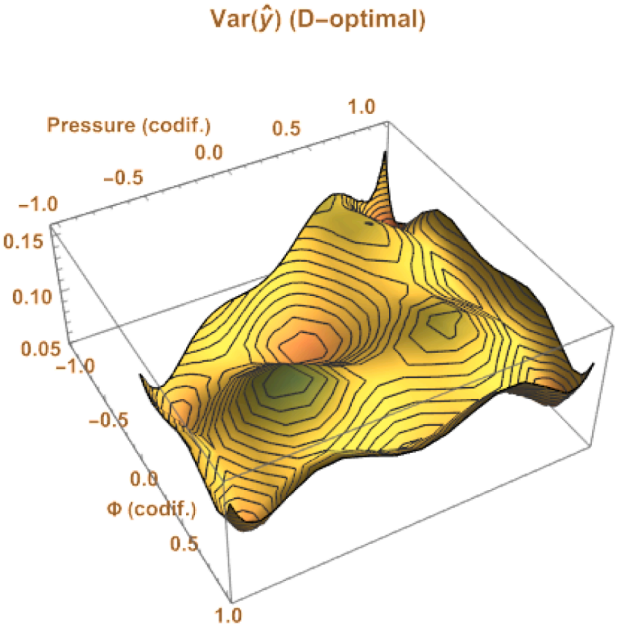

(iii) D-Optimal design - variance

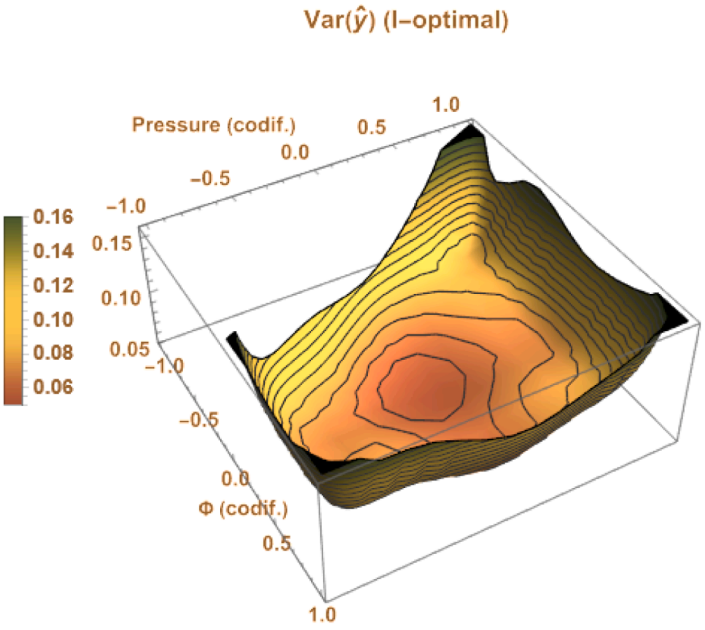

(iv) I-Optimal design -variance

Fig. 5. D- and I-optimal designs for the cubic model.

$$Eff_{\xi}(\eta)=(n_{\xi}/n_{\eta})\ (\Phi\ (M(\xi))/\varphi(M(\eta))), \quad (3)$$

$$Eff_{\xi}(\eta)=(n_{\xi}/n_{\eta})\ (Det\ (M(\eta))/Det\ (M(\xi)))^{1/m} \quad (4)$$

3.2. Choosing the best design

The design space, which is the region where experiments should be made, is defined according to the results obtained from the preliminary samples described previously (Figure 2). The following step decides a model that could describe better the relation between the response variables (t_{trigg_cell}, r_{cell}, t_{max}, t_{comb}, RoUBV, and CCS) and the explanatory variables pressure, p, and fuel/air equivalence ratio (φ). Polynomial models are considered due to the following reasons:

- They are linear models, thus the well-known tool-kit of techniques and algorithms developed for linear models may be used.
- They can locally approximate any general (non-linear) model, leading to the capability of adapting the model. Usually, it is sufficient to use polynomial models up to degree 2 or 3 to get a reasonable approximation.

Finally, a quadratic polynomial model plus pure cubic terms is considered (third order interactions are very rare, thus they were discarded). For ease of computations the explanatory variables are coded to fit in the square [-1,1]x[-1,1] by using the change of variables $X_1=(\Phi -1.1)/0.3$, X2=(P-0.225)/0.075. The number of samples, n, is set at 60, this number is based on the criteria of the time and resources available for experimentation.

Under all these conditions, the optimal experimental design could be obtained. As previously mentioned, there are two main approaches; searching for the best estimation of the model parameters or the best prediction of the response, related to the criteria of D- and I-optimality, respectively. Thus D- and I-optimal designs were obtained using JMP software due to the high number of samples and the restricted design space as shown in Fig. 5, where "codif." means that the pressure as well as the equivalence ratio have been normalized and scaled between -1 and 1.

It can be seen that D-optimal design (Fig. 5i) concentrates more experiments in the edges of the design region, while the I-optimal design (Fig. 5ii) requires more tests in the interior part. In order to compare both designs, an efficiency study was performed, finding that the efficiency of the D-optimal design with respect to I-optimality was 75.5% while the efficiency of the I-optimal design with respect to D-optimality was 87.3 %. From these figures, it deemed more beneficial to choose the I-optimal design because it produces a more accurate prediction of the response and at the same time has a good performance for parameter estimation. Fig. 5iii shows the variance of the response prediction for both designs. It can be clearly observed that the wavering is present in the prediction of the variance for D-optimality (Fig. 5iii showing a number of peaks and valleys in the surface), while a very different behavior is obtained when using the I-optimal design (Fig. 5iv). The latter produces a very flat, almost constant variance, which only increases when approaching to the edges of the region where the I-optimal design places a smaller number of samples.

There is sometimes hesitation about which optimality criteria should be chosen for an experiment. In the cases where there are several candidates, the efficiencies with respect to every criteria can be computed for each design, and then two main approaches can be followed: choosing the design that maximizes a linear combination of the efficiencies (Bayesian optimality), or taking the design that maximizes its minimum efficiency for all the criteria (Minimax criterion), which are related [62]. However, in this case the choice between the two alternatives (D- and I-optimality) seems clear to be I-optimality criteria due to the different efficiencies of the corresponding optimal designs.

3.3. Models for the response parameters

The models obtained for the six cellular parameters (response variables) through the experiments are presented, considering the combination of values of fuel/air equivalence ratio and pressure. Those experiments were given by the 60 point I-optimal design (see Appendix A) where it is possible to see the repetitions of some experiments to verify testing precision and fuel evaporation.

Quadratic polynomial models, in addition to pure cubic terms, are fitted for all the response variables and statistical tests are performed on the parameters modelled. Finally, after removing the non-significant effects, the approximate relations between responses and explanatory variables follow the general form shown in Equation (5). In Table 2 the specific coefficients for each model can be seen. The pressure is in MPa for all the models.

$$Z = \mathbf{A}_1 + \mathbf{A}_2\Phi + \mathbf{A}_3\Phi^2 + \mathbf{A}_4\Phi^3 + \mathbf{A}_5 p + \mathbf{A}_6 p\Phi + \mathbf{A}_7 p^2 \quad (5)$$

For all cellular parameters it is possible to see that the values for the effect of equivalence ratio is greater that of the initial pressure. The coefficients of the quadratic term, followed by the coefficients of the linear term and the coefficients of cubic term are the largest ones, meaning that the value of the equivalence ratio has the most influence on the value of the response parameters. For t_{trigg_cell}, r_{cell} and t_{comb} the difference between the coefficients of the equivalence ratio and those of the pressure is about an order of magnitude, meaning that the pressure has less influence in those coefficients. For those parameters the coefficients of quadratic term of the pressure are very low or, in some cases, even do not exist, verifying the lower influence of the value of the pressure in the different responses.

Nevertheless, for RoUBV and specially for CCS, the coefficients for the equivalence ratio and for the initial pressure are of the same order of magnitude, and then, the quadratic term of the pressure takes importance, which means that the influence of the pressure is comparable to those of the equivalence ratio.

The parameter with the greatest influence on the cellular parameters predicted by the model is the equivalence ratio, rather than the initial pressure, with the exceptions mentioned and within the considered limits.

3.4. Analysis of the models

At this point, the graphical representations of the response models obtained for the cellular parameters are presented and analyzed. Firstly, cellular trigger time and cellular radius are presented in Fig. 6. Then the results of maximum time and combustion duration are presented in Fig. 7 and finally, results of the dimensional parameters are presented in Fig. 8.

Fig. 6i shows the cellular trigger time, t_{trigg_cell} versus the initial pressure and the equivalence ratio obtained by the model developed for the area of study. It can be seen that t_{trigg_cell} is mainly affected by the equivalence ratio, showing the variation of t_{cell} in the domain of the equivalence ratio between 14 ms and 60 ms approximately, while in the pressure domain the variation of t_{trigg_cell} is between 14 ms and 20 ms approximately.

Initially, the equivalence ratio enhances the cellular structure development and the cellular apparition time decreases, until it almost reaches the value of 1.2. For the richest equivalence ratios, it increases, meaning that equivalence ratios higher than 1.2 delays the development of cellularity in the flame. However, the pressure reduces the value of the cellular trigger time for all cases, i.e. the pressure advances the apparition of cellularity.

From the perspective of the equivalence ratio, the minimum values for all the pressures are in the region of $1.1< \varphi <1.2$; t_{trigg_cell} drastically

Table 2
Coefficients of the model according to equivalence ratio and initial pressure.

Cellular parameter (Z)	A_1	A_2	A_3	A_4	A_5	A_6	A_7
t_{trigg_cell} [ms]	−707.91	2197.03	−2237.55	774.59	394.56	−410.88	–
r_{cell} [cm]	−23.41	99.57	−103.79	34.50	−3.09	−4.69	–
t_{max} [ms]	−223.32	919.60	−1115.93	442.28	147.02	−120.80	–
t_{comb} [ms]	−515.46	1731.89	−1912.46	703.59	444.01	−133.59	−602.52
RoUBV	−4.84	20.52	−21.28	7.04	−3.02	−0.94	4.90
CCS	1.43	−6.29	7.82	−2.98	2.23	1.52	−5.96

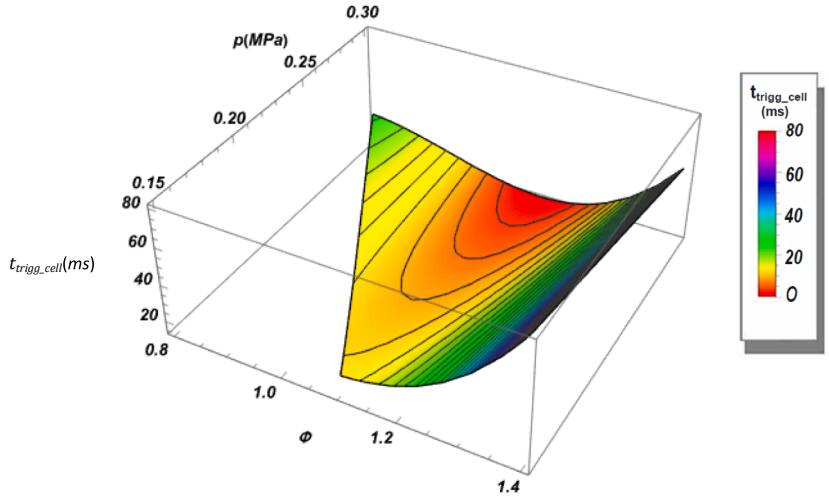

$$\mathbf{t_{trig\_cell}\ [ms]} = -707.91 + 2197.03\Phi - 2237.55\Phi^2 + 774.59\Phi^3 + 394.56p - 410.88p\Phi$$

(i) Cellular trigger time (t_{trigg_cell})

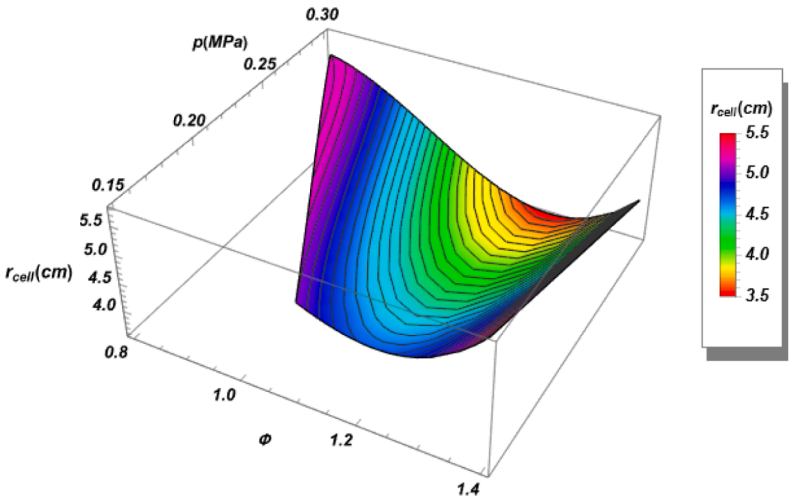

$$\mathbf{r_{cell}\ [cm]} = -23.41 + 99.57\Phi - 103.79\Phi^2 + 34.50\Phi^3 + -3.09p + -4.69p\Phi$$

(ii) Cellular radius (r_{cell})

Fig. 6. Results predicted by the I-optimal DoE for the cellular trigger time (ms) and cellular radius (cm) versus equivalencce ratio and pressure.

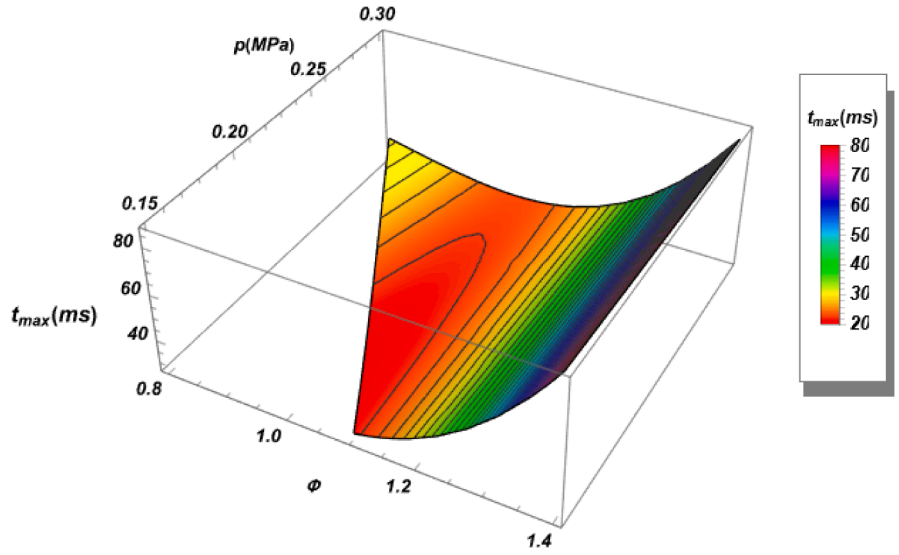

$$\mathbf{t_{max}}\,[ms] = -223.32 + 919.60\Phi - 1115.93\Phi^2 + 442.28\Phi^3 + 147.02\mathrm{p} - 120.80\mathrm{p}\Phi$$

(i) Maximum burning velocity time (t_{ul_max})

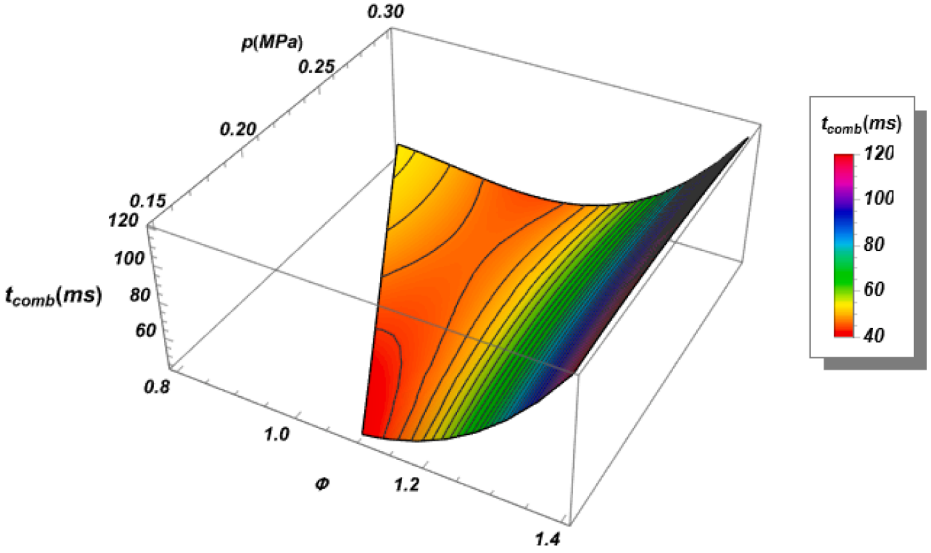

$$\mathbf{t_{comb}}\,[ms] = -515.46 + 1731.89\Phi - 1912.46\Phi^2 + 703.59\Phi^3 + 444.01\mathrm{p} - 133.59\mathrm{p}\Phi - 602.52\mathrm{p}^2$$

(ii) Combustion duration (t_{comb})

Fig. 7. Results predicted by the I-optimal DoE for the maximum burning velocity time and combustion duration versus equivalence ratio and initial pressure.

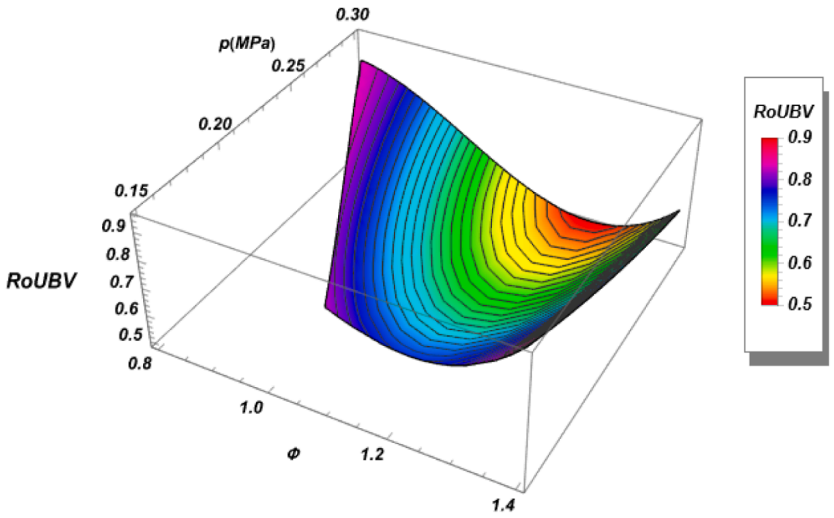

$$\mathbf{RoUBV} = -4.84 + 20.52\Phi - 21.28\Phi^2 + 7.04\Phi^3 - 3.02p - 0.94p\Phi + 4.90p^2$$

(i) Rate of unaffected burning velocity (RoUBV)

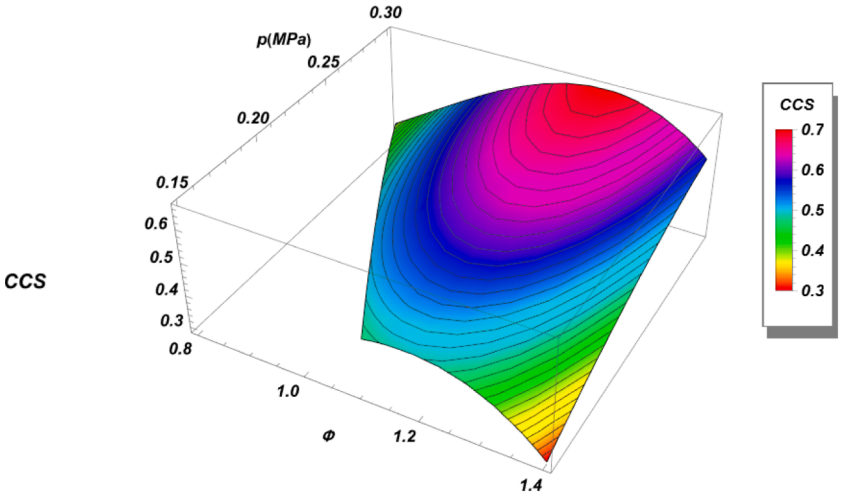

$$CCS = 1.43 - 6.29\Phi + 7.82\Phi^2 - 2.98\Phi^3 + 2.23p + 1.52p\Phi - 5.96p^2$$

(ii) Cellular combustion stage (CCS)

Fig. 8. Results predicted by the I-optimal DoE for the RoUBV and CCS versus equivalence ratio and pressure.

increases for φ >1.2. The absolute minimum of the parameter of the cellular trigger time (t_{trigg_cell}) is located in (φ = 1.15; p = 0.3 MPa) and its value is 14.3 ms.

In summary, in the experiments with smaller t_{trigg_cell}, the cellularity appears earlier in absolute time terms, but it does not necessarily mean that that the cellularity occurs earlier in relative terms. This parameter alone does not allow for the comparison between combustion processes of different initial conditions, as each one has a different total duration, but it is really important for it is the basis of the rest of the cellular parameters obtain in this paper.

In Fig. 6ii it is presented the cellular radius for different values of equivalence ratio and initial pressure, where it is possible to observe the same trend as that noted for the cellular trigger time. In this case, the minimum obtained value is 3.72 cm and it is reached at φ = 1.25, p = 0.3 MPa. On the contrary, for φ = 0.8, p = 0.3 MPa, r_{cell} = 5.4 cm, which means that the onset of the cellularity in this flame occurs when the flame radius has almost reached the combustion chamber diameter (5.7 cm). Even though the highest values of t_{trigg_cell} were reached on the rich side (φ ~1.4), the highest values of r_{cell} are reached on the lean side (φ <1), meaning that the onset of the cellularity occurs early for those conditions.

The minimum value for t_{trigg_cell} and r_{cell} does not happened in the

same conditions, because the first parameter is referred in absolute terms of time (each condition has a different combustion duration), while the second one is expressed in a more relative way (because all of them has the same maximum radius 5.7 cm, the radius of the combustion chamber), which allows to compare the cellular radius for different conditions.

In Fig. 7 are represented the response surfaces for t_{comb}, which represents the duration of the combustion process, and t_{ul_max}, which represents the time at which the process reaches the maximum value of the burning velocity, are now considered. Although these two values represent different time instants, their values are directly related: a greater t_{ul_max} or greater t_{comb} means that the flame front takes longer to consume the unburned mixture, obtaining lower burning velocity. However, t_{comb} is always greater than t_{ul_max} because when the maximum velocity is reached, kinetic reactions are still taking place. Similarly to t_{trigg_cell} and r_{cell}, t_{max} and t_{comb} seem to be influenced mainly by the equivalence ratio, rather than the initial pressure (see Fig. 6).

Fig. 7i shows the surface that encompasses the values of t_{ul_max} for the area of study according to φ and p_i. Here, the pressure has a positive influence in both parameters, because their values increase with the pressure. The minimum value of t_{max} is 28.91 ms for $\varphi = 1.1$, $p_i = 0.15$ MPa, and the minimum of t_{comb} is 43.47 ms also for $\varphi = 1.1$ and $p_i = 0.15$ MPa, as can be seen in Fig. 7ii. Both parameters have a similar behavior with respect to equivalence ratio and pressure, meaning that the maximum values are in the rich side at φ=1.4 for ethanol combustion.

These two parameters, t_{ul_max} and t_{comb}, combined with t_{trigg_cell} create additional information insight to the cellular behavior of the flames. The relationship between these parameters allows the comparison between experiments and gives an idea of when the cellular flame is developed in terms of the stage of combustion (in relative terms and not absolute terms like t_{trigg_cell}).

In Fig. 8 are presented results for the dimensionless parameters obtained with the I-optimal DoE, in Fig. 8i, the evolution of the RoUBV versus equivalence ratio and initial pressure is shown. It is observed that the RoUBV for the equivalence ratios from 0.8 to 1.2 decreases, due to the early appearance of cellularity, and therefore the part of the laminar burning velocity that is not affected by the cellular effect decreases to a minimum for an equivalence ratio of 1.2 approximately. From this value, the appearance of the cellular structure is delayed again, and therefore the laminar burning velocity stage increases. It is also possible to observe that even though the influence of φ is stronger than that of p, the influence of the initial pressure on RoUBV is higher than the parameters studied before.

This effect can be seen in Fig. 8 and inferred from Table 2 of the coefficients because RoUBV depends on the quadratic term of initial pressure. The figure has a similar shape to that of r_{cell}. The minimum value of this parameter is 0.489 for φ =1.24 and p=0.3 MPa. These conditions produce the maximum difference between the onset of cellularity (t_{trigg_cell}) and the time when the flame is most affected by the cellularity (t_{ul_max}); i.e., in this point, the cellularity has more time to develop because the difference between t_{trigg_cell} and t_{max} is a maximum. On the contrary, for those combustion processes at lean conditions, RoUBV is maximum, implying that the burning velocity is unaffected a greater portion of time, and therefore the cellularity has little time to develop. The contrary (1-RoUBV) would represent the portion of time during which the cellularity develops, until the maximum burning velocity time, when it occurs its maximum development, in terms of influence in the burning velocity.

In Fig. 8ii it is shown the graph for Cellular Combustion Stage (CCS) according to the initial pressure (in MPa) and the equivalence ratio obtained by the model presented for the region of study. As seen with RoUBV, the influence of the initial pressure is greater than the parameters presented before. The maximum of the CCS parameter is 0.668 for φ =1.21 and p=0.3 MPa. This means that the cellularity starts to develop once the combustion process is 33.2% complete, with 100% representing the condition when all the unburned gas is consumed. This parameter represents the percentage of the combustion (in time terms) affected by the presence of cellularity in the flame front.

4. Results

This section presents the experimental results obtained from the I-optimal design experiments and their relationship to the predictive models introduced in the previous section; also, the schlieren images for ethanol flames are shown.

4.1. Relation between the models proposed and the images obtained

The coherence between the cellular parameters obtained by the models and the Schlieren images obtained experimentally under certain conditions are now considered. The goal of this analysis is to confirm with the appearance of the cellularity in the images if the models can predict correctly that instant; another secondary goal is if the cellular parameters could define other characteristics of the cellularity.

For this analysis a group of three experiments is selected in which the equivalence ratio is fixed and the initial pressure changes. The conditions as well as the cellular parameters obtained by the models are presented in Table 3.

Fig. 9 shows the corresponding images to the cellular radius for each one of the conditions exposed in Table 3. The images on the left column are for a radius 0.5 cm smaller than the cellular one, and, parallelly, the images on the right column are 0.5 cm greater than the cellular one. The comparation between those images allows to study qualitatively the evolution and morphology of the cellularity.

Observing the images in Fig. 9, the cellularity in Fig. 9i is a homogeneous cellularity, while in (iii) is observed a heterogeneous shape due to the previous growth of the cracks near the electrodes. Cellularity in (ii) could be considered a transition between (i) and (iii). In the radius that the model considers cellular, in all the cases, it can be seen the initial changes in the shape of the flame morphology due to the cellularity beginning, which is starting to develop. In the previous image cellularity cannot be appreciated under any conditions and in the subsequent image it can be seen a completely cellular flame front is developed. Both the models for cellular radius and cellular trigger time can predict correctly the apparition of the cellularity in those images. Case (i), with an equivalence ratio of 1.26, has the lowest RoUBV (under 0.7) and the highest CCS (above 0.5) of all three, also has the lowest cellular radius. Those parameters could identify this type of cellularity. The cases of (i) and (iii) have similar values of r_{cell}, RoUBV and CCS, which means that only with the value of absolute times (t_{trigg_cell}, t_{max} or t_{comb}) the two of them could be differentiated: the heterogeneous cellularity in (iii) has the greater absolute times.

In a previous work developed by Reyes et al. [10], these cellularity morphologies (homogeneous or heterogeneous) were already observed and investigated, ford the conclusion was that they were related to the type of instabilities that were responsible of the cellularity. Fist image of Fig. 9iii shows a homogeneous cellular flame with a defined spherical shape, since there are not noticeable wrinkles in the surface and the cells

Table 3
Cellular parameters of the models for different equivalence ratio and 0.195 MPa of initial pressure.

	a φ = 1.01; p = 0.195 MPa	b φ = 1.26; p = 0.195 MPa	c φ = 1.40; p = 0.195 MPa
t_{trigg_cell} [ms]	23.092	33.422	72.674
r_{cell} [cm]	5.356	4.534	5.351
t_{ul_max} [ms]	27.738	47.432	86.193
t_{comb} [ms]	45.179	68.788	118.611
RoUBV	0.850	0.678	0.836
CCS	0.478	0.534	0.392

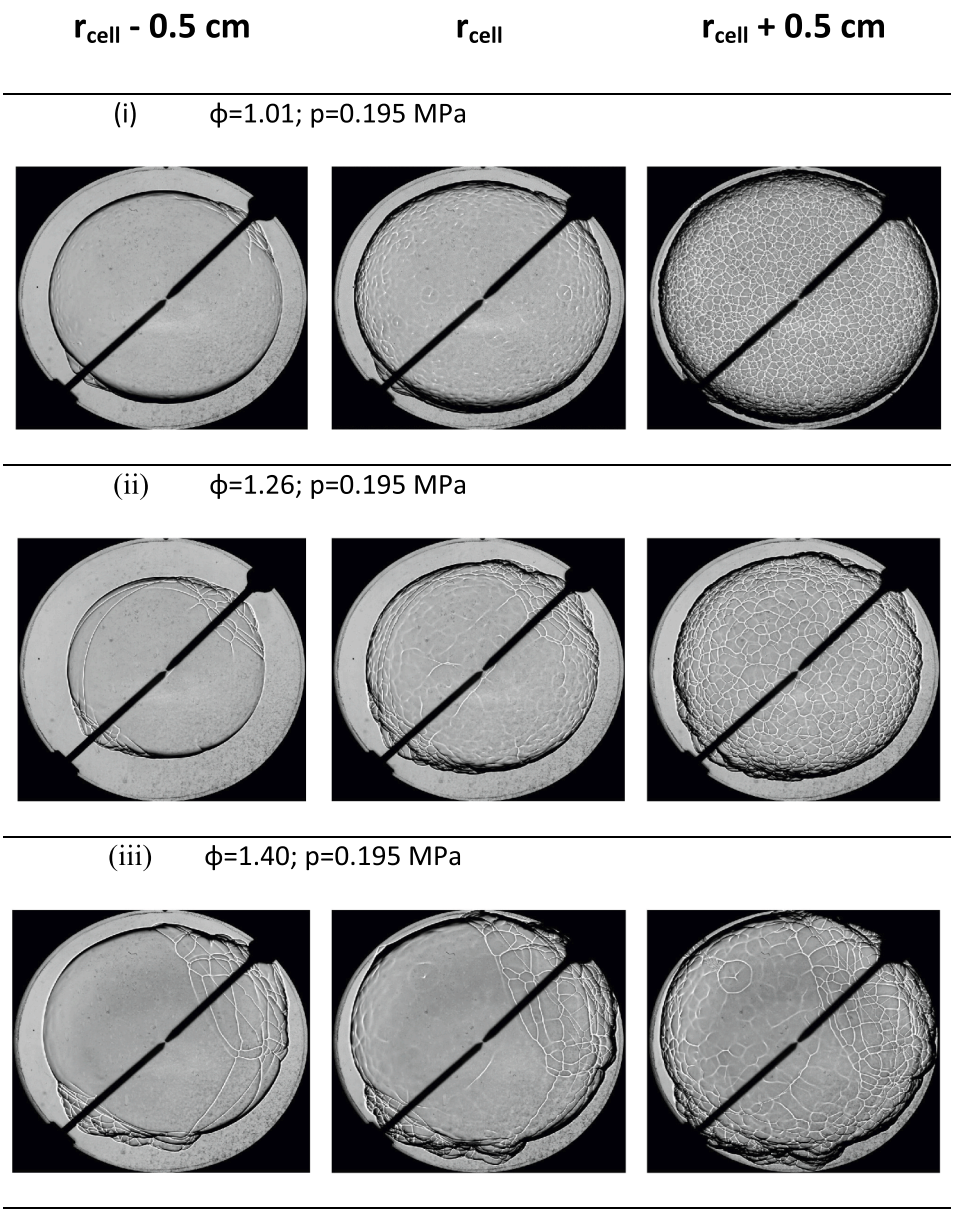

Fig. 9. Schlieren images during the cellularity appearance under three different conditions.

Table 4
Cellular parameters of the models for an equivalence ratio equal to 1.24 and 0.262 MPa of initial pressure.

	φ=1.24; p=0.262 MPa
t_{trigg_cell} [ms]	22.721
r_{cell} [cm]	3.92
t_{max} [ms]	43.66
t_{comb} [ms]	64.533
RoUBV	0.544
CCS	0.635

are homogeneously spread and this kind of morphology is associated with the hydrodynamic effect. Third image of Fig. 9iii contains a cellular flame front structure with large-scale wrinkles as well as smaller scale cells, which leads to a clustered aspect to the flame front; this kind of morphology is associated with the thermal-diffusive effect, as it is detailed in ref [10].

To verify that low RoUBV of high CCS can identify combustions with a cellularity of transition between a homogeneous and heterogeneous one, another experiment is studied. Its conditions and its cellular parameters are in Table 4.

Analyzing only the cellular parameter, it is seen that the RoUBV is under 0.7, as the combustion of 0.195 MPa and 1.01 of equivalence ratio in Table 4. Also, the CCS is more than 0.5, which means that more than the 50% of the combustion process is affected by the cellularity. These parameters indicate that is a cellularity of transition. Also, the cellular radius is small. This is confirmed by the images shown next in Fig. 10. There are some cracks before the cellular radius and the cells are not completely homogeneous after the cellular radius, due to the combined action of hydrodynamic and thermal-diffusive effects. A more extensive analysis is required to quantify the contribution of both effects to the cellular morphology and study the origin and nature of the instabilities developed in ethanol spherical flames.

The images verify that the model predicts correctly the cellular radius, when the cellularity starts to modify the flame front. Also, this confirms that the cellularity affects the burning velocity in the way that was exposed in the first section of this paper.

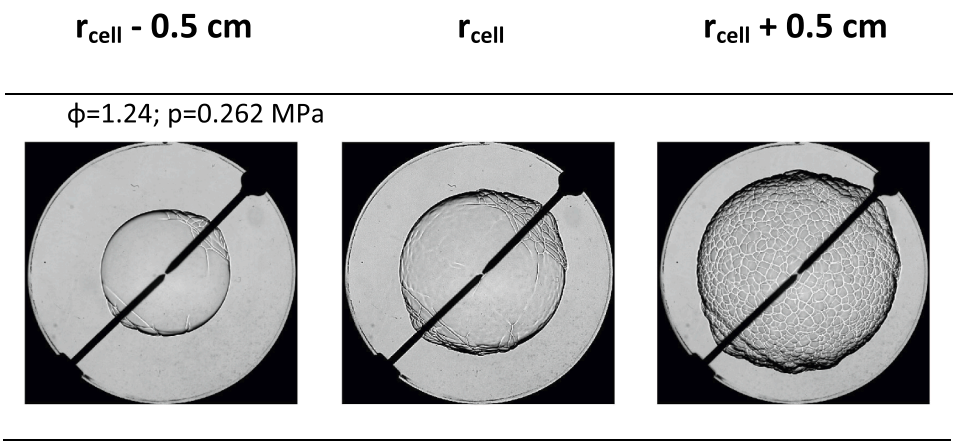

Fig. 10. Schlieren images during the cellularity appearance for φ = 1.24; p = 0.262 MPa.

4.2. Comparation with literature

Once it has been verified that the I-optimal model predictions are consistent with the experimental results shown through the images, in this section, present results are compared with those obtained by other authors. The cellular radius is the most calculated cellular parameter in the bibliography to study the appearance of the cellularity in spherical flames. The work of Zhang et al. [35] carried out a theoretical investigation of instabilities in ethanol flames. This work is used to compare and validate present work results. In that paper, Zhang et al. [35] calculated the cellular radius (what they called critical radius) applying the theory of instabilities that was mentioned in the first section of present work.

Fig. 11 shows the plot where the present results of the model and experiments are compared with the theoretical results of Zhang et al. The dotted lines correspond to the study of Zhang et al., while the continuous lines are referred to present work results for cellular radius. The points are present results obtained directly from the experiments (with the corresponding uncertainty). The black color is associated with 0.2 MPa approximately, the purple is 0.3 MPa and the orange is 0.5 MPa. Zhang et al. did not obtain results for 0.3 MPa.

The global trend for the cellular radius is the same for both works. Zhang et al. did not give explicit information about the equation that relates the cellular radius, the pressure and the equivalence ratio, but their results could be approximated to a polynomial curve with an equivalence ratio cubic term (φ^3) for a R^2=0.98 for both pressures. This is the same dependency as in the model for the cellular radius presented in Table 2.

The 0.5 MPa curves are not as well fitted as the ones that correspond to 0.2 MPa. This could be because the model of the present work for cellular radius is calculated for a range of pressure that goes from 0.15 MPa to 0.3 MPa. Even so, the global tendency is the same, for the higher the initial pressure is, the smaller the critical radius are.

The curves of 0.2 MPa fit adequately for rich equivalence ratios and slightly disagree in near stoichiometric ones, where the theory underestimates the value for the cellular radius. The highest error in this condition is about 12% between 1 and 1.1, which is not a very big difference considering that theoretical and experimental results are

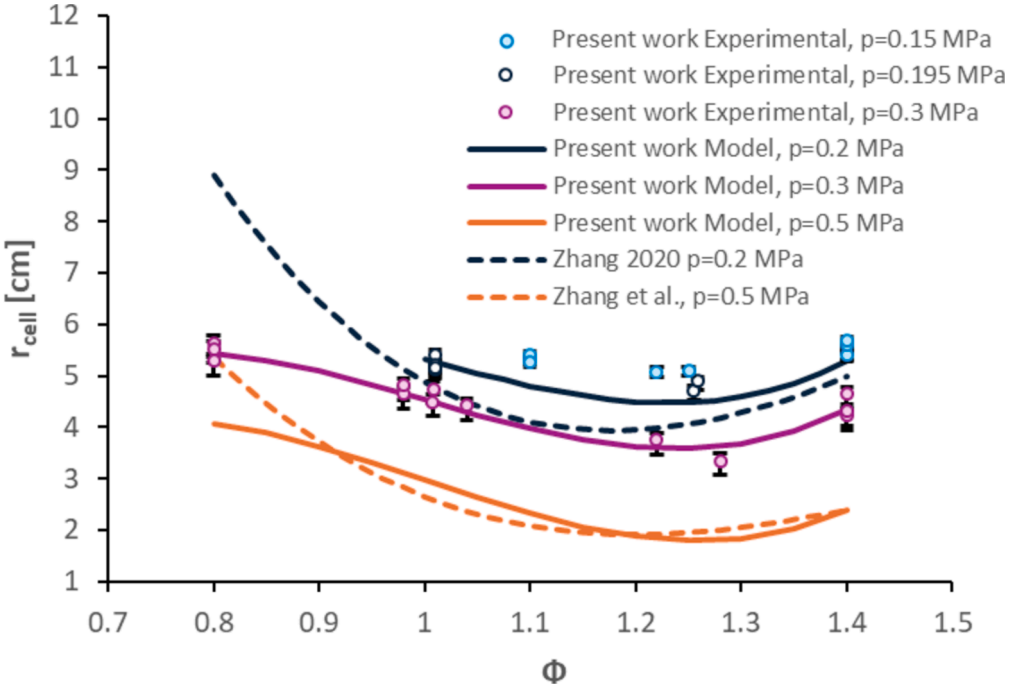

Fig. 11. Comparation between the cellular radius given by the model and experiments of the present work and those obtained by Zhang et al.

compared. The results for 0.3 MPa are placed between 0.2 MPa and 0.5 MPa which perfectly agrees with the study of Zhang et al. that says that the pressure reduce the value of the cellular radius. As a conclusion of this section, it can be said that the predictions of cellular radius obtained with present model are in accordance with the results obtained by Zhang et al. [35].

5. Conclusions

In this work, an experimental analysis of the apparition of cellular structures in premixed, laminar ethanol flames was conducted together with an I-optimal design of experiments. Experiments were performed for different initial conditions of pressure and equivalence ratio in a cylindrical constant volume combustion bomb in order to characterize the apparition of cellularity caused by instabilities developed in the flame front during the ethanol combustion.

Experimental tests have been developed using a statistical design of experiments tool which allows not only for the design of experimental conditions to test, but also the reduction of the number of required conditions to predict the evolution of response parameters (so-called cellular parameters) that characterize the appearance of cellularity. The chosen design of experiments is an I-optimal design, which allows for a lower variance of the predicted response while keeping a low variance of the estimators of the model parameters.

Six cellular parameters were proposed to analyze cellularity emergence. The dimensional parameters were: Cellular trigger time (t_{trigg_cell}), cellular radius (r_{cell}), maximum burning velocity time (t_{ul_max}) and combustion duration (t_{comb}), while the dimensionless parameters were proposed to characterize the appearance of the cellularity in a relative way: Ratio of Unaffected Burning Velocity (RoUBV) and Cellular Combustion Stage (CCS).

The main conclusions of the experimental trends are summarized as follows: equivalence ratio is the main factor influencing the appearance of the cellular structure, followed by initial pressure. Pressure enhances the instabilities development, i.e., for a higher initial pressure, the range equivalence ratio that develops a cellular structure becomes wider. The latter is concluded considering the limits of equivalence ratio and initial pressure between the experiments developed within the study: $\varphi \in (0.8; 1,4)$ and $p \in (1.5; 3)$ bar.

Maximum values of cellular radius and rate of unaffected burning velocity are obtained in the lean side and for the maximum initial pressure, while combustion with a longer stage of cellular development is obtained for higher initial pressures and equivalence ratios near to 1.2.

The predicted models of the cellular parameters were compared to the images results, concluding that the models can predict the beginning of the cellularity in the flame. Indirectly, this means that the instant of acceleration of the burning velocity was a good criterion for establishing the cellular trigger time. The model has been also proven to give more information about the morphology of the cellularity in a general way, for it was observed that the cellularity did not take always the same morphology, and it was related with the values of the cellular parameters. Finally, the model for the cellular radius was validated by comparing with results obtained in literature.

In a future work, it is necessary to study the instabilities growth rate to analyze the origin of the instabilities that cause the different types of cellular morphologies. Furthermore, it would be interesting to determine the effect in the cellularity of initial temperature and the addition of other fuels as hydrogen.

From the point of view of design and modelling, an extension of this work could include the study of the relationship between the response variables and consider the corresponding multi-response model.

CRediT authorship contribution statement

R. Sastre: Writing – original draft, Methodology, Investigation, Conceptualization. **M. Reyes:** Writing – original draft, Validation, Supervision, Methodology, Investigation, Formal analysis, Conceptualization. **J.M. Rodríguez-Díaz:** Writing – original draft, Validation, Software, Data curation. **J. Lacey:** Writing – review & editing, Supervision, Investigation.

Declaration of competing interest

The authors declare that they have no known competing financial interests or personal relationships that could have appeared to influence the work reported in this paper.

Acknowledgements

The authors would like to thank the Spanish Ministry of Science and Innovation-Agencia Estatal de Investigación, for the financial support of this investigation with the research project PID2019-106957RB-C22. This work was developed under the support of the Research Group in Engines and Renewable Energies (MyER) from the University of Valladolid. The authors would like to thank to the University of Valladolid (Spain) for financial support through the pre-doctoral contract CONTPR-2022-500. This research was partially supported by the Spanish Ministry of Science, Innovation and Universities project PID2021-125211OB-I00 and by the Junta de Castilla y León project 'SA217P23' (J.M. R-D).

Appendix A

1-Optimal design used in the experiment

Equivalence ratio, φ	Pressure, p (MPa)	Equivalence ratio, φ	Pressure, p (MPa)	Equivalence ratio, φ	Pressure, p (MPa)
0.80	0.300	1.01	0.195	1.26	0.195
0.80	0.300	1.01	0.195	1.26	0.193
0.80	0.300	1.04	0.300	1.26	0.192
0.89	0.255	1.10	0.150	1.26	0.194
0.89	0.254	1.10	0.150	1.26	0.194
0.89	0.254	1.10	0.150	1.26	0.193
0.98	0.300	1.22	0.150	1.26	0.195
0.98	0.30	1.22	0.300	1.28	0.300
0.99	0.264	1.23	0.260	1.40	0.257
0.99	0.265	1.23	0.261	1.40	0.261
1.00	0.264	1.23	0.258	1.40	0.150
1.00	0.264	1.24	0.262	1.40	0.150
1.00	0.265	1.24	0.261	1.40	0.150

(continued on next page)

(*continued*)

Equivalence ratio, φ	Pressure, p (MPa)	Equivalence ratio, φ	Pressure, p (MPa)	Equivalence ratio, φ	Pressure, p (MPa)
1.00	0.266	1.24	0.261	1.40	0.192
1.01	0.300	1.24	0.261	1.40	0.195
1.01	0.300	1.24	0.260	1.40	0.195
1.01	0.195	1.24	0.262	1.40	0.255
1.01	0.195	1.24	0.195	1.40	0.300
1.01	0.195	1.25	0.150	1.40	0.300
1.01	0.195	1.26	0.195	1.40	0.300

Data availability

Data will be made available on request.

References

[1] Astbury GR. A review of the properties and hazards of some alternative fuels. Process Saf Environ Protect 2008;86(6):397–414. https://doi.org/10.1016/j.psep.2008.05.001.

[2] Reyes M, Tinaut FV, Giménez B, Pastor JV. Effect of hydrogen addition on the OH* and CH* chemiluminescence emissions of premixed combustion of methane-air mixtures. Int J Hydrogen Energy 2018;43(42):19778–91. https://doi.org/10.1016/j.ijhydene.2018.09.005.

[3] Tinaut FV, Reyes M, Melgar A, Giménez B. Optical characterization of hydrogen-air laminar combustion under cellularity conditions. Int J Hydrogen Energy 2019;44(25):12857–71. https://doi.org/10.1016/j.ijhydene.2018.11.134.

[4] Okafor EC, et al. Experimental and numerical study of the laminar burning velocity of CH4–NH3–air premixed flames. Combust Flame 2018;187:185–98. https://doi.org/10.1016/j.combustflame.2017.09.002.

[5] Lhuillier C, Brequigny P, Lamoureux N, Contino F, Mounaïm-Rousselle C. Experimental investigation on laminar burning velocities of ammonia/hydrogen/air mixtures at elevated temperatures. Fuel Mar. 2020;263. https://doi.org/10.1016/j.fuel.2019.116653.

[6] Wang D, Ji C, Wang Z, Wang S, Zhang T, Yang J. Measurement of oxy-ammonia laminar burning velocity at normal and elevated temperatures. Fuel Nov. 2020;279. https://doi.org/10.1016/j.fuel.2020.118425.

[7] Xia Y, et al. Turbulent burning velocity of ammonia/oxygen/nitrogen premixed flame in O2-enriched air condition. Fuel 2020;268:117383. https://doi.org/10.1016/j.fuel.2020.117383.

[8] Horváth IS, Tabatabaei M, Karimi K, Kumar R. Recent updates on biogas production – a review. Biofuel Res J 3(2). Green Wave Publishing of Canada; 2016. pp. 394–402. doi: 10.18331/BRJ2016.3.2.4.

[9] Zabed H, Sahu JN, Suely A, Boyce AN, Faruq G. Bioethanol production from renewable sources: current perspectives and technological progress. Renew Sustain Energy Rev May 2017;71:475–501. https://doi.org/10.1016/J.RSER.2016.12.076.

[10] Reyes M, Sastre R, Tinaut FV, Rodríguez-Fernández J. Study and characterization of the instabilities generated in expanding spherical flames of hydrogen/methane/air mixtures. Int J Hydrogen Energy 2022;7:22616–32. https://doi.org/10.1016/j.ijhydene.2022.05.063.

[11] Reyes M, Sastre R, Giménez B, Sesma C. Experimental, kinetic modeling and morphologic study of the premixed combustion of hydrogen/methane mixtures. Energies (Basel) 2022;15(10):3722. https://doi.org/10.3390/en15103722.

[12] Reyes M, Tinaut FV, Horrillo A, Lafuente A. Experimental characterization of burning velocities of premixed methane-air and hydrogen-air mixtures in a constant volume combustion bomb at moderate pressure and temperature. Appl Therm Eng Feb. 2018;130:684–97. https://doi.org/10.1016/j.applthermaleng.2017.10.165.

[13] Hu E, Huang Z, He J, Zheng J, Miao H. Measurements of laminar burning velocities and onset of cellular instabilities of methane-hydrogen-air flames at elevated pressures and temperatures. Int J Hydrogen Energy 2009;34(13):5574–84. https://doi.org/10.1016/j.ijhydene.2009.04.058.

[14] Huang S, Huang R, Zhang Y, Zhou P, Wang Z, Yin Z. Relationship between cellular morphology and self-acceleration in lean hydrogen-air expanding flames. Int J Hydrogen Energy 2019;44(59):31531–43. https://doi.org/10.1016/j.ijhydene.2019.09.229.

[15] huan Jiang Y, xiu Li G, meng Li H, peng Zhang G, cheng Lv J. Experimental study on the influence of hydrogen fraction on self-acceleration of H2/CO/air laminar premixed flame. Int J Hydrogen Energy 2020;45(3):2351–2359. doi: 10.1016/j.ijhydene.2019.11.044.

[16] Yang S, Saha A, Wu F, Law CK. Morphology and self-acceleration of expanding laminar flames with flame-front cellular instabilities. Combust Flame Sep. 2016;171:112–8. https://doi.org/10.1016/J.COMBUSTFLAME.2016.05.017.

[17] Kim W, Sato Y, Johzaki T, Endo T, Shimokuri D, Miyoshi A. Experimental study on self-acceleration in expanding spherical hydrogen-air flames. Int J Hydrogen Energy Jul. 2018;43(27):12556–64. https://doi.org/10.1016/j.ijhydene.2018.04.153.

[18] Robert E, Monkewitz PA. Thermal-diffusive instabilities in unstretched, planar diffusion flames. Combust Flame 2012;159(3):1228–38.

[19] Matalon M. Intrinsic flame instabilities in premixed and nonpremixed combustion. Annu Rev Fluid Mech 2007;39:163–91. https://doi.org/10.1146/annurev.fluid.38.050304.092153.

[20] Oppong F, Luo Z, Li X, Song Y, Xu C. Intrinsic instability of different fuels spherically expanding flames: a review. Fuel Process Technol Sep. 2022;234:107325. https://doi.org/10.1016/J.FUPROC.2022.107325.

[21] Markstein GH. Experimental and theoretical studies of flame-front stability, P. B. T.-D. of C. F. Pelcé, Ed., San Diego: Academic Press; 1950. doi: 10.1016/B978-0-08-092523-3.50045-9.

[22] Clavin P. Dynamic behavior of premixed flame fronts in laminar and turbulent flows. Prog Energy Combust Sci 1985;11(1):1–59. https://doi.org/10.1016/0360-1285(85)90012-7.

[23] Williams FA. Combustion Theory. The Fundamental Theory of Chemically Reacting Flow Systems, Second. California: Princeton University; 1985.

[24] Bechtold JK, Matalon M. Hydrodynamic and diffusion effects on the stability of spherically expanding flames. Combust Flame 1987;67(1):77–90. https://doi.org/10.1016/0010-2180(87)90015-0.

[25] Bradley D, Sheppart CGW, Woolley R, Greenhalgh DA, Lockett RD. The development and structure of flame instabilities and cellularity at low Markstein numbers in explosions. Combust Flame 2000;122(1–2):195–209. https://doi.org/10.1016/S0010-2180(00)00113-9.

[26] Addabbo R. The structure and stabilitty of expanding and convering near-stoichimetric flames. [PhD Thesis], New Jersey's Science and Technology University, Newark, New Jersey; 2001.

[27] Law CK, Jomaas G, Bechtold JK. Cellular instabilities of expanding hydrogen/propane spherical flames at elevated pressures: theory and experiment. Proc Combust Inst 2005;30(1):159–67. https://doi.org/10.1016/j.proci.2004.08.266.

[28] Addabbo R, Bechtold JK, Matalon M. Wrinkling of spherically expanding flames. Proc Combust Inst 2002;29(2):1527–35. https://doi.org/10.1016/s1540-7489(02)80187-0.

[29] Kwon OC, Rozenchan G, Law CK. Cellular instabilities and self-acceleration of outwardly propagating spherical flames. Proc Combust Inst 2002;29(2):1775–83. https://doi.org/10.1016/S1540-7489(02)80215-2.

[30] Jomaas G, Law CK, Bechtold JK. On transition to cellularity in expanding spherical flames. J Fluid Mech 2007;583:1–26. https://doi.org/10.1017/S0022112007005885.

[31] Li T, et al. Investigation on hydrogen/ethanol intrinsic flame instability. Combust Flame 2022;241:112064. https://doi.org/10.1016/j.combustflame.2022.112064.

[32] Oppong F, Zhongyang L, Li X, Xu C. Inherent instabilities in ethyl acetate premixed flames. Fuel 2021;290(December):2020. https://doi.org/10.1016/j.fuel.2020.120000.

[33] Wu H, Zheng J, Dong X, Zhang S, Ding Y. Investigations on the cellular instabilities of expanding hydrogen/methanol spherical flame. Int J Hydrogen Energy 2021;46(67):33601–15. https://doi.org/10.1016/j.ijhydene.2021.07.194.

[34] Li X, Wang Q, Oppong F, Liu W, Xu C. Cellularization characteristics of ethyl acetate spherical expanding flame. Fuel May 2021;291:120213. https://doi.org/10.1016/J.FUEL.2021.120213.

[35] Zhang N, et al. Numerical and theoretical investigation of ethanol/air flame instability. Combust Theor Model 2020;24(6):1108–29. https://doi.org/10.1080/13647830.2020.1820578.

[36] Liu F, et al. Numerical study and cellular instability analysis of E30-air mixtures at elevated temperatures and pressures. Fuel 2019;271(November):2020. https://doi.org/10.1016/j.fuel.2020.117458.

[37] Kim HJ, Van K, Lee DK, Yoo CS, Park J, Chung SH. Laminar flame speed, Markstein length, and cellular instability for spherically propagating methane/ethylene–air premixed flames. Combust Flame 2020;214:464–74. https://doi.org/10.1016/j.combustflame.2020.01.011.

[38] Wang Z. Experimental and theoretical studies of laminar burning speed and flame instability of alternative fuels and refrigerants. [PhD Thesis], Northeastern University, Boston, Massachusetts; 2020.

[39] Hinton NID. Measuring laminar burning velocities using constant volume combustion vessel technique. [PhD Thesis], University of Oxford, Michaelmas; 2014.

[40] Giménez B, Melgar A, Horrillo A, Tinaut F. Combustion speed in ICE: thermodynamic model for combustion speed, expansion speed, data base. Mendeley Data, V1, 2019. doi: 10.17632/wskmmkg6rk.1.

[41] Gárzon Lama LFM, Pizzuti L, Sotton J, Martins CA. Experimental investigation of hydrous ethanol/air flame front instabilities at elevated temperature and pressures. Fuel 2021;287(November):2020. https://doi.org/10.1016/j.fuel.2020.119555.

[42] López-Fidalgo J, Rodríguez-Díaz JM. Characteristic polynomial criteria in optimal experimental design BT - MODA 5 — advances in model-oriented data analysis and

experimental design. A.C. Atkinson, L. Pronzato, and H. P. Wynn, Eds., Heidelberg: Physica-Verlag HD; 1998. p. 31–38.
[43] Rodríguez-Díaz JM, López-Fidalgo J. Optimal characteristic designs for polynomial models BT - optimum design 2000. In: Atkinson A, Bogacka B, Zhigljavsky A, Eds., Boston, MA: Springer US, 2001, pp. 123–130. doi: 10.1007/978-1-4757-3419-5_12.
[44] Rodríguez-Díaz JM, López-Fidalgo J. A bidimensional class of optimality criteria involving φp and characteristic criteria. Statistics (Ber) Jul. 2003;37(4):325–34. https://doi.org/10.1080/0233188031000112863.
[45] Elfving G. Optimum allocation in linear regression theory. Ann Math Stat Jun. 1952;23(2):255–62. https://doi.org/10.1214/aoms/1177729442.
[46] López-Fidalgo J, Rodríguez-Díaz JM. Elfving's method for m-dimensional models. Metrika 2004;59(3):235–44. https://doi.org/10.1007/s001840300281.
[47] Rodríguez-Díaz JM. Computation of c-optimal designs for models with correlated observations. Comput Stat Data Anal 2017;113:287–96. https://doi.org/10.1016/j.csda.2016.10.019.
[48] Rodríguez-Díaz JM, Sánchez-León G. Design optimality for models defined by a system of ordinary differential equations. Biom J 2014;56(5):886–900.
[49] Pukelsheim F. Optimal design of experiments. Soc Ind Appl Math 2006.
[50] Atkinson A, Donev A, Tobias R. Optimum Experimental Designs, With SAS. Oxford: Oxford University Press; 2007.
[51] Fedorov VV, Hackl P. Model-oriented design of experiments. vol. 125. Springer Science & Business Media; 2012.
[52] Bradley D, Lawes M, Mansour MS. Explosion bomb measurements of ethanol–air laminar gaseous flame characteristics at pressures up to 1.4 MPa. Combust Flame Jul. 2009;156(7):1462–70. https://doi.org/10.1016/J.COMBUSTFLAME.2009.02.007.
[53] Reyes M, Pérez JF, Sastre R. Combustion performance and flame front morphology of producer gas from a biomass gasification-based cookstove. Fuel 2023;362 (December):2024. https://doi.org/10.1016/j.fuel.2023.130763.
[54] Bychkov VV, Liberman MA. Dynamics and stability of premixed flames. Phys Rep 2000;325(4):115–237. https://doi.org/10.1016/S0370-1573(99)00081-2.
[55] Nawaz B et al. Optical characterization of cellular instabilities in spherically expanding ammonia-hydrogen flames; 2023. pp. 1–11.
[56] Lapalme D, Halter F, Mounaïm-Rousselle C, Seers P. Characterization of thermodiffusive and hydrodynamic mechanisms on the cellular instability of syngas fuel blended with CH4 or CO2. Combust Flame Jul. 2018;193:481–90. https://doi.org/10.1016/j.combustflame.2018.03.028.
[57] Zhang G, et al. Deep learning-driven analysis for cellular structure characteristics of spherical premixed hydrogen-air flames. Int J Hydrogen Energy May 2024;68: 63–73. https://doi.org/10.1016/j.ijhydene.2024.04.232.
[58] Tinaut FV, Melgar A, Giménez B, Reyes M. Prediction of performance and emissions of an engine fuelled with natural gas/hydrogen blends. Int J Hydrogen Energy 2011;36(1):947–56. https://doi.org/10.1016/j.ijhydene.2010.10.025.
[59] Kenward MG, Roger JH. Small sample inference for fixed effects from restricted maximum likelihood. Biometrics 1997;53(3):983–97.
[60] Kenward MG, Roger JH. An improved approximation to the precision of fixed effects from restricted maximum likelihood. Comput Stat Data Anal 2009;53(7): 2583–95.
[61] Rodríguez-Díaz JM, Rivas-López MJ, Martín-Chaves S, Vereas-Talaván C. Optimal designs for random blocks model using corrected criteria. Qual Reliab Eng Int 2016;32(5):1707–14.
[62] Tommasi C, Rodríguez-Díaz JM, López-Fidalgo JF. An equivalence theorem for design optimality with respect to a multi-objective criterion. Stat Pap 2023;64(4): 1041–56.
[63] Qiyang Wang, Yang Song, Kai Liu, Xiaolu Li, Cangsu Xu, Laminar "Combustion characteristics of methane/methanol/air mixtures: Experimental and kinetic investigations. Case Stud Thermal Eng 2023;41, 102593, ISSN 2214-157X, doi: 10.1016/j.csite.2022.102593.